frontiers | Frontiers in Neural Circuits

TYPE Original Research
PUBLISHED 21 February 2023
DOI 10.3389/fncir.2023.1121049

OPEN ACCESS

EDITED BY
Artur Kania,
Montreal Clinical Research Institute (IRCM), Canada

REVIEWED BY
Isabel Martinez Garay,
Cardiff University, United Kingdom
Paschalis Kratsios,
The University of Chicago, United States
Fadel Tissir,
Hamad Bin Khalifa University, Qatar

*CORRESPONDENCE
Polyxeni Philippidou
✉ pxp282@case.edu

RECEIVED 11 December 2022
ACCEPTED 06 February 2023
PUBLISHED 21 February 2023

CITATION
Vagnozzi AN, Moore MT, López de Boer R, Agarwal A, Zampieri N, Landmesser LT and Philippidou P (2023) Catenin signaling controls phrenic motor neuron development and function during a narrow temporal window.
Front. Neural Circuits 17:1121049.
doi: 10.3389/fncir.2023.1121049

Catenin signaling controls phrenic motor neuron development and function during a narrow temporal window

Alicia N. Vagnozzi[1], Matthew T. Moore[1], Raquel López de Boer[1], Aambar Agarwal[1], Niccolò Zampieri[2], Lynn T. Landmesser[1] and Polyxeni Philippidou[1]*

[1]Department of Neurosciences, Case Western Reserve University, Cleveland, OH, United States, [2]Max Delbrück Center for Molecular Medicine in the Helmholtz Association (MDC), Berlin, Germany

Phrenic Motor Column (PMC) neurons are a specialized subset of motor neurons (MNs) that provide the only motor innervation to the diaphragm muscle and are therefore essential for survival. Despite their critical role, the mechanisms that control phrenic MN development and function are not well understood. Here, we show that catenin-mediated cadherin adhesive function is required for multiple aspects of phrenic MN development. Deletion of β- and γ-*catenin* from MN progenitors results in perinatal lethality and a severe reduction in phrenic MN bursting activity. In the absence of catenin signaling, phrenic MN topography is eroded, MN clustering is lost and phrenic axons and dendrites fail to grow appropriately. Despite the essential requirement for catenins in early phrenic MN development, they appear to be dispensable for phrenic MN maintenance, as catenin deletion from postmitotic MNs does not impact phrenic MN topography or function. Our data reveal a fundamental role for catenins in PMC development and suggest that distinct mechanisms are likely to control PMC maintenance.

KEYWORDS

cadherins, catenins, respiratory, phrenic motor neurons, breathing

Introduction

Breathing is an essential motor behavior that is required for survival. In mammals, contraction of the diaphragm muscle is critical for bringing oxygenated air into the lungs during inspiration (Greer, 2012). Diaphragm contractions are mediated by a specialized subset of motor neurons (MNs), Phrenic Motor Column (PMC) neurons that reside in the cervical spinal cord and project their axons along the phrenic nerve in the thoracic cavity to reach the diaphragm. Phrenic MNs exhibit distinct properties from other MN subtypes, including tight clustering and stereotyped axonal and dendritic morphologies. While they are derived from a common MN progenitor domain, phrenic MNs acquire their unique features through the activity of a selective transcriptional program that distinguishes them from other MNs (Philippidou et al., 2012; Machado et al., 2014; Chaimowicz et al., 2019; Vagnozzi et al., 2020). Phrenic-specific transcription factors (TFs) initiate and maintain the expression of a distinct set of genes, including a unique combination of cell surface adhesion

molecules (Machado et al., 2014; Vagnozzi et al., 2020). While many of these molecular markers show specific and sustained expression in phrenic MNs, their functions in phrenic MN development and maintenance have not been tested.

We previously identified a distinct combinatorial cadherin code that defines phrenic MNs, which includes both the broadly expressed type I N-cadherin and a subset of specific type II cadherins (Vagnozzi et al., 2020, 2022). Cadherins are calcium-dependent transmembrane cell adhesion molecules that interact with cytosolic catenin proteins to induce changes in the actin cytoskeleton, thus regulating many neuronal processes such as migration, topography, and morphology (Seong et al., 2015). For example, cadherins regulate cortical neuron migration (Martinez-Garay, 2020), hippocampal dendritic growth and branching (Esch et al., 2000; Yu and Malenka, 2003; Bekirov et al., 2008), as well as dendrite morphogenesis and arborization within the visual and olfactory systems (Riehl et al., 1996; Masai et al., 2003; Zhu and Luo, 2004; Tanabe et al., 2006; Hirano and Takeichi, 2012; Duan et al., 2018). In the spinal cord, cadherins engage β- and γ-catenins to establish the segregation and settling position of MN cell bodies (Price et al., 2002; Demireva et al., 2011; Dewitz et al., 2018, 2019). β-catenin is required in muscle for neuromuscular junction (NMJ) formation and function, however it appears to act redundantly with γ-catenin in MNs, as only joint β- and γ-catenin inactivation leads to disorganization of MN subtypes, including PMC neurons (Li et al., 2008; Demireva et al., 2011; Vagnozzi et al., 2020). However, it is unknown whether β- and γ-catenins have additional roles in phrenic MN development and function, and whether they continue to be required after initial PMC topography has been established.

Here, we show that catenin activity is required for proper respiratory behavior and robust respiratory output. After MN-specific deletion of β- and γ-*catenin*, mice display severe respiratory insufficiency, gasp for breath, and die within hours of birth. Using phrenic nerve recordings, we determined that catenins are crucial for respiratory motor output, as MN-specific catenin inactivation leads to a striking decrease in phrenic MN activity. We further show that catenins are required to establish phrenic MN cell body settling position, as well as PMC axonal and dendritic morphology. Finally, we show that catenins are only required for PMC development and function during a narrow developmental window, as catenin deletion from postmitotic MNs does not impact respiratory output. Our data demonstrate a fundamental role for the cadherin-catenin cell adhesion complex in phrenic MN development and respiratory function and indicate that distinct pathways likely act to maintain PMC function.

Materials and methods

Mouse genetics

The β-*catenin* (Brault et al., 2001) and γ-*catenin* (Demireva et al., 2011) alleles, *Olig2::Cre* (Dessaud et al., 2007) and *ChAT::Cre* (Lowell et al., 2006) lines were generated as previously described and maintained on a mixed background. Mouse colony maintenance and handling was performed in compliance with protocols approved by the Institutional Animal Care Use Committee of Case Western Reserve University. Mice were housed in a 12-h light/dark cycle in cages containing no more than five animals at a time.

Immunohistochemistry and *in situ* hybridization

In situ hybridization and immunohistochemistry was performed as previously described (Philippidou et al., 2012; Vagnozzi et al., 2020), on tissue fixed for 2 h in 4% paraformaldehyde (PFA) and cryosectioned at 16 μm. *In situ* probes were generated from e12.5 cervical spinal cord cDNA libraries using PCR primers with a T7 RNA polymerase promoter sequence at the 5' end of the reverse primer. All probes generated were 750–1000 bp in length. Wholemounts of diaphragm muscles were stained as described (Philippidou et al., 2012). The following antibodies were used: rabbit anti-cleaved Caspase 3 (1:1000; Cell Signaling, RRID:AB_2341188), mouse anti-olig2-A488-conjugated (1:500; Millipore, RRID:AB_11205039), rabbit anti-β-Catenin (1:250; Cell Signaling Technology, RRID:AB_11127203), goat anti-Scip (1:5000; Santa Cruz Biotechnology, RRID:AB_2268536), mouse anti-Islet1/2 (1:1000, DSHB, RRID:AB_2314683) (Tsuchida et al., 1994), rabbit anti-neurofilament (1:1000; Synaptic Systems, RRID:AB_887743), rabbit anti-synaptophysin (1:250, Thermo Fisher, RRID:AB_10983675), and α-bungarotoxin Alexa Fluor 555 conjugate (1:1000; Invitrogen, RRID:AB_2617152). Images were obtained with a Zeiss LSM 800 confocal microscope and analyzed with Zen Blue, ImageJ (Fiji), and Imaris (Bitplane). Phrenic MN number was quantified using the Imaris "spots" function to detect cell bodies that coexpressed high levels of Scip and Isl1/2 in a region of interest limited to the left and right sides of the ventral spinal cord.

DiI tracing

For labeling of phrenic MNs, crystals of carbocyanine dye, DiI (Invitrogen, #D3911) were pressed onto the phrenic nerves of eviscerated embryos at e18.5, and the embryos were incubated in 4% PFA at 37°C in the dark for 4–5 weeks. Spinal cords were then dissected, embedded in 4% low melting point agarose (Invitrogen) and sectioned using a Leica VT1000S vibratome at 100–150 μm.

Positional analysis

MN positional analysis and correlation analysis were performed as previously described (Dewitz et al., 2018, 2019). MN positions were acquired using the "spots" function of the imaging software Imaris (Bitplane) to assign x and y coordinates. Coordinates were expressed relative to the midpoint of the spinal cord midline, defined as position $x = 0$, $y = 0$. To account for experimental variations in spinal cord size, orientation, and shape, sections were normalized to a standardized spinal cord whose dimensions were empirically calculated at e13.5 (midline to the lateral edge = 390 μm). We analyzed every other section containing the entire PMC (20–30 s in total per embryo).

Dendritic orientation analysis

For the analysis of dendritic orientation, we superimposed a radial grid divided into eighths (45° per octant) centered over phrenic MN cell bodies spanning the entire length of the dendrites. We drew a circle around the cell bodies and deleted the fluorescence associated with them. Fiji (ImageJ) was used to calculate the fluorescent intensity (IntDen) in each octant which was divided by the sum of the total fluorescent intensity to calculate the percentage of dendritic intensity in each area.

Electrophysiology

Electrophysiology was performed as previously described (Vagnozzi et al., 2020). Mice were cryoanesthetized and rapid dissection was carried out in 22–26°C oxygenated Ringer's solution. The solution was composed of 128 mM NaCl, 4 mM KCl, 21 mM $NaHCO_3$, 0.5 mM NaH_2PO_4, 2 mM $CaCl_2$, 1 mM $MgCl_2$, and 30 mM D-glucose and was equilibrated by bubbling in 95% O_2/5% CO_2. The hindbrain and spinal cord were exposed by ventral laminectomy, and phrenic nerves exposed and dissected free of connective tissue. A transection at the pontomedullary boundary rostral to the anterior inferior cerebellar artery was used to initiate fictive inspiration. Electrophysiology was performed under continuous perfusion of oxygenated Ringer's solution from rostral to caudal. Suction electrodes were attached to phrenic nerves just proximal to their arrival at the diaphragm. The signal was band-pass filtered from 10 Hz to 3 kHz using AM-Systems amplifiers (Model 3000), amplified 5,000-fold, and sampled at a rate of 50 kHz with a Digidata 1440A (Molecular Devices). Data were recorded using AxoScope software (Molecular Devices) and analyzed in Spike2 (Cambridge Electronic Design). Burst duration and burst activity were computed from 4 to 5 bursts per mouse, while burst frequency was determined from 10 or more minutes of recording time per mouse. Burst activity was computed by rectifying and integrating the traces with an integration time equal to 2 s, long enough to encompass the entire burst. The maximum amplitude of the rectified and integrated signal was then measured and reported as the total burst activity.

Plethysmography

Conscious, unrestrained P0 mice were placed in a whole body, flow-through plethysmograph (emka) attached to a differential pressure transducer (emka). We modified 10 ml syringes to use as chambers, as smaller chambers increase signal detection in younger mice. Experiments were done in room air (79% nitrogen, 21% oxygen). Mice were placed in the chamber for 30 s at a time, for a total of three to five times, and breathing parameters were recorded. Mice were directly observed to identify resting breaths. At least ten resting breaths were analyzed from every mouse. Data are presented as fold control, where the control is the average of 2 littermates in normal air.

Experimental design and statistical analysis

For all experiments a minimum of three embryos per genotype, both male and female, were used for all reported results unless otherwise stated. The Shapiro–Wilk test was used to determine normality. All data, with the exception of electrophysiology burst activity data in **Figures 2**, **6**, showed normal distribution and *p*-values were calculated using unpaired, two-tailed Student's *t*-test. Burst activity data in **Figures 2**, **6** showed non-normal distribution and *p*-values were calculated using the Mann–Whitney test. $p < 0.05$ was considered to be statistically significant, where $^{*}p < 0.05$, $^{**}p < 0.01$, $^{***}p < 0.001$, and $^{****}p < 0.0001$. Data are presented as box and whisker plots with each dot representing data from one mouse unless otherwise stated. Small open squares in box and whisker plots represent the mean.

Results

Catenin signaling is required for survival, proper respiratory behavior, and phrenic MN activation

Phrenic MNs express a distinct combinatorial cadherin code (Machado et al., 2014; Vagnozzi et al., 2020), but the collective contribution of these molecules to phrenic MN development, maintenance and function has not been established. We previously found that phrenic MNs express the type I *N-cadherin* (*N-cad*) and the type II cadherins *Cdh6, 9, 10, 11*, and *22* (Vagnozzi et al., 2020). To investigate the role of cadherin signaling in phrenic MN development, we previously eliminated cadherin signaling in MN progenitors by inactivating β- and γ-*catenin* using a *Olig2::Cre* promoter (β-*catenin flox/flox;* γ-*catenin flox/-; Olig2::Cre*). β- and γ-catenin are obligate intracellular factors required for cadherin-mediated cell adhesive function and catenin deletion enables us to interrogate the full repertoire of cadherin actions in phrenic MNs (**Figure 1A**). We found that loss of β- and γ-*catenin* led to phrenic MN disorganization, however we were unable to assess the role of catenins in respiratory behavior and function as these mice die by e14.5 (Vagnozzi et al., 2020). Therefore, we modified our genetic strategy and generated β-*catenin flox/flox;* γ-*catenin flox/flox; Olig2::Cre* mice, referred to as βγ-$cat^{MN\Delta}$ mice. βγ-$cat^{MN\Delta}$ mice show loss of β- and γ-catenin in both MN progenitors and MNs (expressing the TF Isl1/2) by e11.5 (**Supplementary Figure 1A**). We find that βγ-$cat^{MN\Delta}$ mice are born alive but die within 24 h of birth and often display severe flexion of the wrist joint (**Figure 1B**).

In order to assess breathing in βγ-$cat^{MN\Delta}$ mice, we utilized unrestrained whole body flow-through plethysmography at postnatal day (P)0 (**Figure 1C**). We found that βγ-$cat^{MN\Delta}$ mice have a 45% reduction in tidal volume (the amount of air inhaled during a normal breath), while respiratory frequency is not affected (**Figures 1D, E**). This results in an average 45% reduction in overall air drawn into the lungs per minute (minute

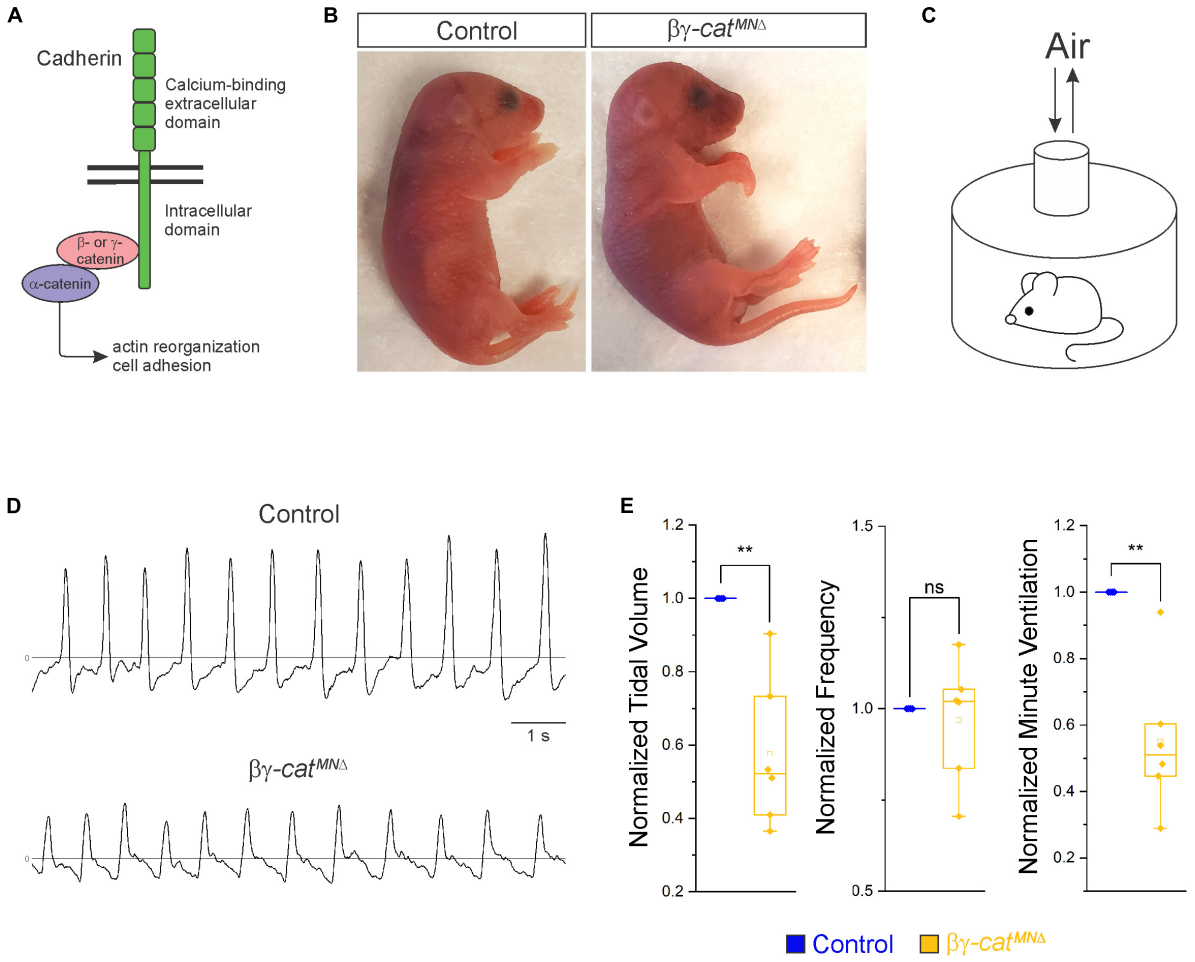

FIGURE 1
Catenin signaling is required for survival and proper respiratory behavior. **(A)** B- and γ-catenin are obligate intracellular factors required for cadherin-mediated cell adhesive function. We utilized inactivation of β- and γ-catenin in MNs (β-*catenin flox/flox;* γ-*catenin flox/flox; Olig2::Cre,* referred to as βγ-*cat*$^{MN\Delta}$ mice) as a strategy to define the function of cadherin signaling in phrenic MNs. **(B)** Appearance of P0 control and βγ-*cat*$^{MN\Delta}$ mice. *B*γ-*cat*$^{MN\Delta}$ mice are cyanotic and die shortly after birth. **(C)** Experimental setup for whole body plethysmography experiments. **(D)** Representative 10 s traces in room air from control and βγ-*cat*$^{MN\Delta}$ mice at P0. **(E)** βγ-*cat*$^{MN\Delta}$ mice display reduced tidal volume resulting in a 45% reduction in overall ventilation ($n = 4$ control, $n = 6$ βγ-*cat*$^{MN\Delta}$ mice). $^{**}p < 0.01$.

ventilation, Figure 1E), indicating βγ-*cat*$^{MN\Delta}$ mice likely die from respiratory failure. Our findings indicate that catenin signaling is necessary for proper respiratory behavior and survival. To further examine respiratory circuitry intrinsic to the brainstem and spinal cord, we performed suction recordings of the phrenic nerve in isolated brainstem-spinal cord preparations (Figure 2A). These preparations display fictive inspiration after the removal of inhibitory networks in the pons *via* transection, and thus represent a robust model to interrogate circuit level changes. We examined whether catenin deletion impacts circuit output at embryonic day (e)18.5/P0, shortly before βγ-*cat*$^{MN\Delta}$ mice die. We observed a striking reduction in the activation of phrenic MNs in βγ-*cat*$^{MN\Delta}$ mice (Figure 2B). While bursts in control mice exhibit large peak amplitude, bursts in βγ-*cat*$^{MN\Delta}$ mice were either of very low amplitude (∼85%) or non-detectable (∼15%). After rectifying and integrating the traces, we found a nearly 70% decrease in total burst activity in βγ-*cat*$^{MN\Delta}$ mice (Figure 2C). Our data indicate that cadherin signaling is imperative for robust activation of phrenic MNs during inspiration.

Catenins establish phrenic MN topography and organization

What accounts for the loss of phrenic MN activity in βγ-*cat*$^{MN\Delta}$ mice? We asked whether early phrenic MN specification, migration and survival are impacted after catenin inactivation. We acquired transverse spinal cord sections through the entire PMC at e11.5 and stained for the TF Olig2 to label MN progenitors and the phrenic-specific TF Scip and MN-specific TF Isl1/2 to label all phrenic MNs (Supplementary Figure 1B). We found that MN progenitor numbers do not change in βγ-*cat*$^{MN\Delta}$ mice. However, their distribution along the dorsoventral axis is altered, indicating that catenin signaling is not required for MN progenitor generation but is necessary for progenitor restricted localization within a narrow band (Supplementary Figures 1B, C). We found a cluster of Scip+ MNs in the ventral cervical spinal cord of both control and βγ-*cat*$^{MN\Delta}$ mice, indicating that early phrenic MN specification is unperturbed (Supplementary Figure 1B). βγ-*cat*$^{MN\Delta}$ mice show a non-significant reduction of phrenic MNs

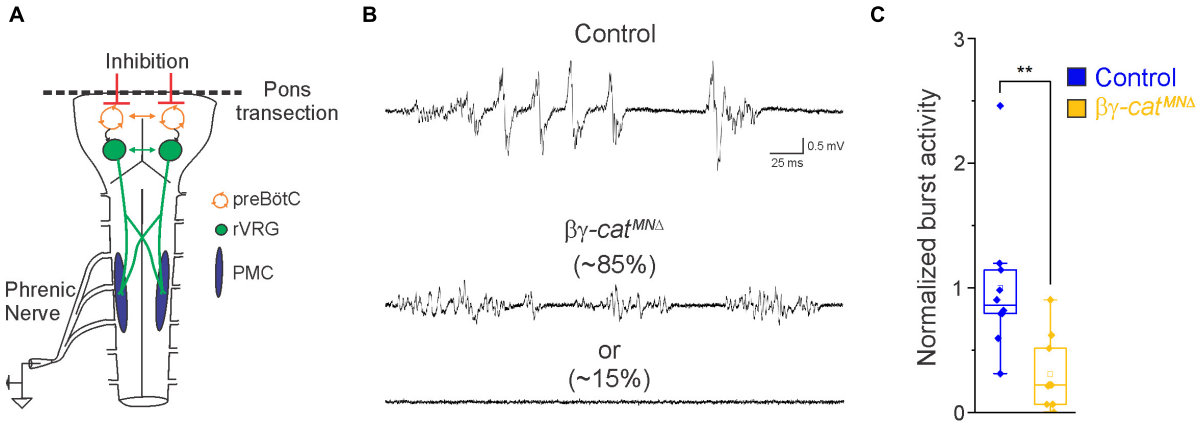

FIGURE 2
Catenin signaling controls phrenic MN activation. **(A)** Schematic of brainstem-spinal cord preparation, which displays fictive inspiration after removal of the pons. Suction electrode recordings were taken from the phrenic nerve in the thoracic cavity at e18.5/P0. **(B)** Enlargement of single respiratory bursts reveals a reduction in burst amplitude and overall activity in βγ-$cat^{MN\Delta}$ mice. Partial (initial 350 ms) bursts are shown. While 85% of βγ-$cat^{MN\Delta}$ mice display respiratory bursts, 15% show no bursts throughout the recording period. **(C)** βγ-$cat^{MN\Delta}$ mice exhibit nearly 70% reduction in burst activity ($n = 10$ control, $n = 10$ βγ-$cat^{MN\Delta}$ mice). $^{**}p < 0.01$.

at e11.5 (Supplementary Figure 1C). However, we observed a significant reduction in phrenic MN numbers by e13.5 in βγ-$cat^{MN\Delta}$ mice, indicating that catenin signaling is necessary for phrenic MN survival (Figures 3A, B). While we do not observe a significant increase in activated caspase 3 levels in βγ-$cat^{MN\Delta}$ mice at e11.5, it is possible that the relatively high levels of apoptosis at this stage mask the increase in cell death in the relatively small phrenic MN population (Supplementary Figures 1B, C).

While phrenic MNs are normally distributed along the rostrocaudal axis, we found that they sometimes show migratory defects, where several phrenic MNs remain close to the midline instead of fully migrating (Figure 3C, arrow), and also appear to shift both ventrally and medially in βγ-$cat^{MN\Delta}$ mice. To quantitate PMC cell body position, each phrenic MN was assigned a cartesian coordinate, with the midpoint of the spinal cord midline defined as (0,0). Bγ-$cat^{MN\Delta}$ mice displayed a significant shift in phrenic MN cell body position, with cell bodies shifting ventrally toward the edge of the spinal cord and toward the midline (Figures 3C–F). We quantified the average ventrodorsal and mediolateral phrenic MN position per embryo and found a significant change in phrenic MN position in both axes in βγ-$cat^{MN\Delta}$ mice (Figure 3G). Correlation analysis indicated that control and βγ-$cat^{MN\Delta}$ mice are dissimilar from each other ($r = 0.47$, Figure 3H), indicating that catenins establish phrenic MN coordinates during development.

In addition to changes in cell body position, we also noticed that phrenic MNs appear to lose their tight clustering in βγ-$cat^{MN\Delta}$ mice. PMC clustering is thought to be critical for the proper development of the respiratory system because it facilitates recruitment of motor units through electrical coupling in the embryo to compensate for weak inspiratory drive (Greer and Funk, 2005). In order to determine PMC clustering defects, we used Imaris to measure the average distance between phrenic MNs. We found that βγ-$cat^{MN\Delta}$ mice had a nearly 50% increase in the average distance between neighboring cells (Figure 3I), indicating that the cadherin/catenin adhesive complex contributes to the formation of a tightly clustered phrenic motor column.

Catenins are required for phrenic MN dendrite and axon growth

Since cadherin/catenin signaling is imperative for phrenic MN organization, we also asked whether any other aspects of phrenic MN development, such as dendritic and axon growth, might rely on catenin actions. We examined dendritic orientation in control and βγ-$cat^{MN\Delta}$ mice by injecting the lipophilic dye dil into the phrenic nerve at e18.5 (Figure 4A). DiI diffuses along the phrenic nerve to label both PMC cell bodies and dendrites. Consistent with our earlier observations, we found that phrenic cell bodies are often scattered in βγ-$cat^{MN\Delta}$ mice. Interestingly, even phrenic MNs that are significantly displaced correctly project along the phrenic nerve (arrows, Figure 4A), indicating that changes in cell body position do not impact axon trajectory choice. In control mice, phrenic MN dendrites branch out in dorsolateral to ventromedial directions; in βγ-$cat^{MN\Delta}$ mice, however, they exhibit stunted growth, defasciculation and a failure to extend in the dorsolateral direction (Figure 4A).

To quantify these changes, we superimposed a radial grid divided into octants onto the dendrites and measured the fluorescent intensity in each octant after removal of any fluorescence associated with the cell bodies. Zero degrees was defined by a line running perpendicular from the midline through the center of cell bodies. In control mice, the majority of dendrites project in the dorsolateral direction (0–90°), representing 40–45% of the overall dendritic intensity (Figures 4B, D, E). Ventrally projecting dendrites (180–225° and 315–360°) were also prominent, giving rise to nearly 30% of the overall dendritic intensity (Figures 4B, D, E). We found that catenin deletion resulted in a striking reduction in dorsolateral dendrites, together with a significant increase in ventral dendrites (Figures 4C–E), indicating that cadherins are necessary for establishing phrenic MN dendritic orientation. These changes in phrenic dendritic topography in βγ-$cat^{MN\Delta}$ mice may impact their targeting by

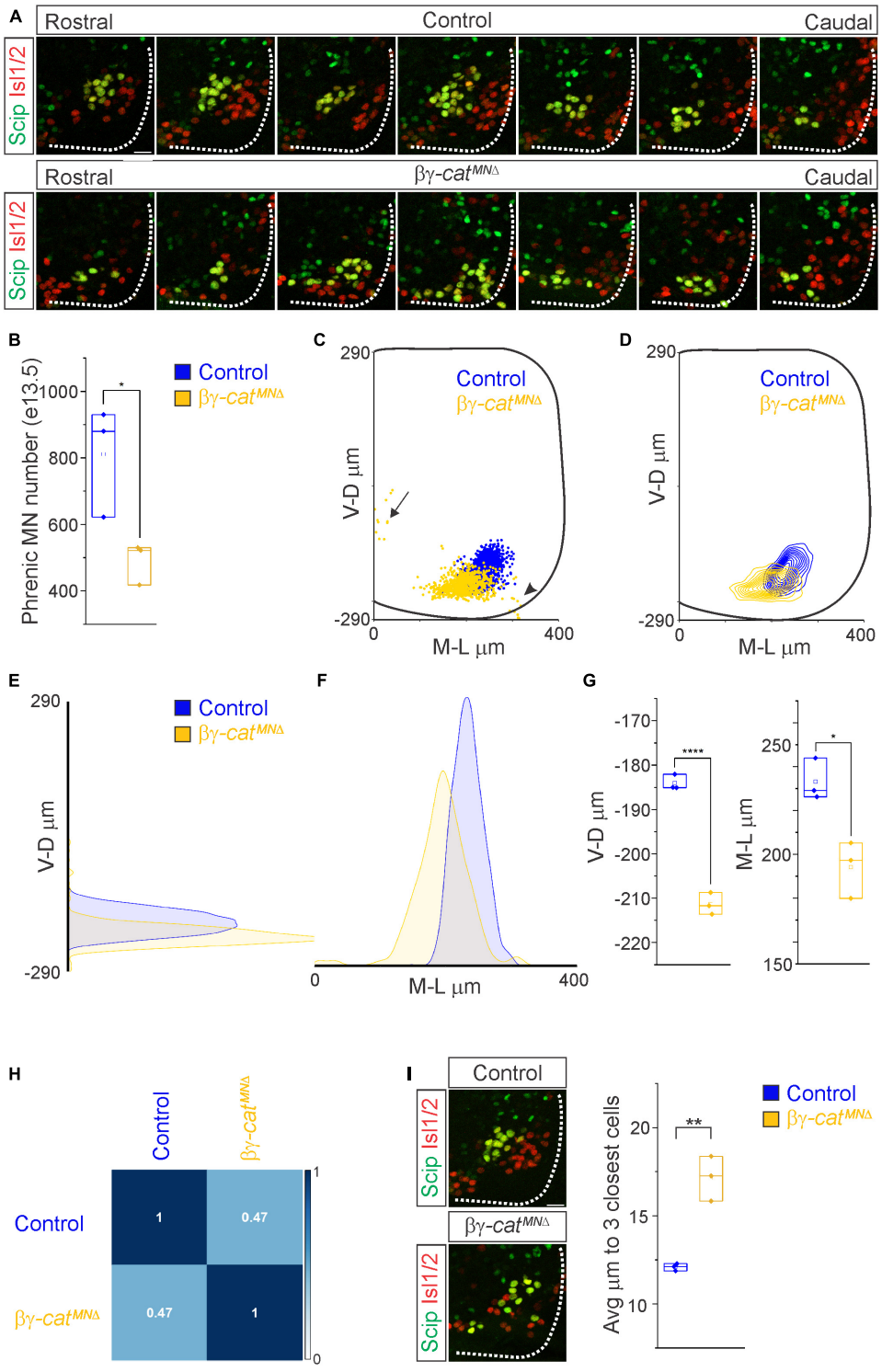

FIGURE 3
Catenins establish phrenic MN topography and organization. **(A)** Rostral to caudal distribution of e13.5 phrenic MN cell bodies (yellow, defined by the expression of Scip in green and Isl1/2 in red) in control and βγ-*cat*^{MNΔ} mice. While phrenic MN cell bodies in control mice gradually shift toward more ventral positions at caudal locations, phrenic cell bodies are located ventrally in βγ-*cat*^{MNΔ} mice even at rostral levels. In addition, cell bodies in βγ-*cat*^{MNΔ} mice appear less clustered. **(B)** Reduction in phrenic MN number in βγ-*cat*^{MNΔ} mice. **(C)** Reconstructed distribution of cell bodies in control and βγ-*cat*^{MNΔ} mice. Occasional cell bodies remain near the progenitor zone in βγ-*cat*^{MNΔ} mice (arrow), while others seem to be dragged out of the spinal cord by their axon (arrowhead). **(D)** Contour density plot of phrenic cell body position in control and βγ-*cat*^{MNΔ} mice at e13.5. V-D µm; ventrodorsal position, M-L µm; mediolateral position. (0,0) represents the center of the spinal cord in both dimensions. Density plots of ventrodorsal **(E)** and mediolateral **(F)** cell body position in control and βγ-*cat*^{MNΔ} mice. **(G)** Quantification of ventrodorsal and mediolateral position, showing significant shifts in βγ-*cat*^{MNΔ} mice. **(H)** Correlation analysis of phrenic MN positional coordinates in control and βγ-*cat*^{MNΔ} mice. Zero is no correlation, while 1 is a perfect correlation. **(I)** Phrenic MNs have an increased average distance to their neighboring phrenic MNs in βγ-*cat*^{MNΔ} mice, indicating loss of clustering. Scale bar = 25 µm. *$p < 0.05$, **$p < 0.01$, and ****$p < 0.0001$.

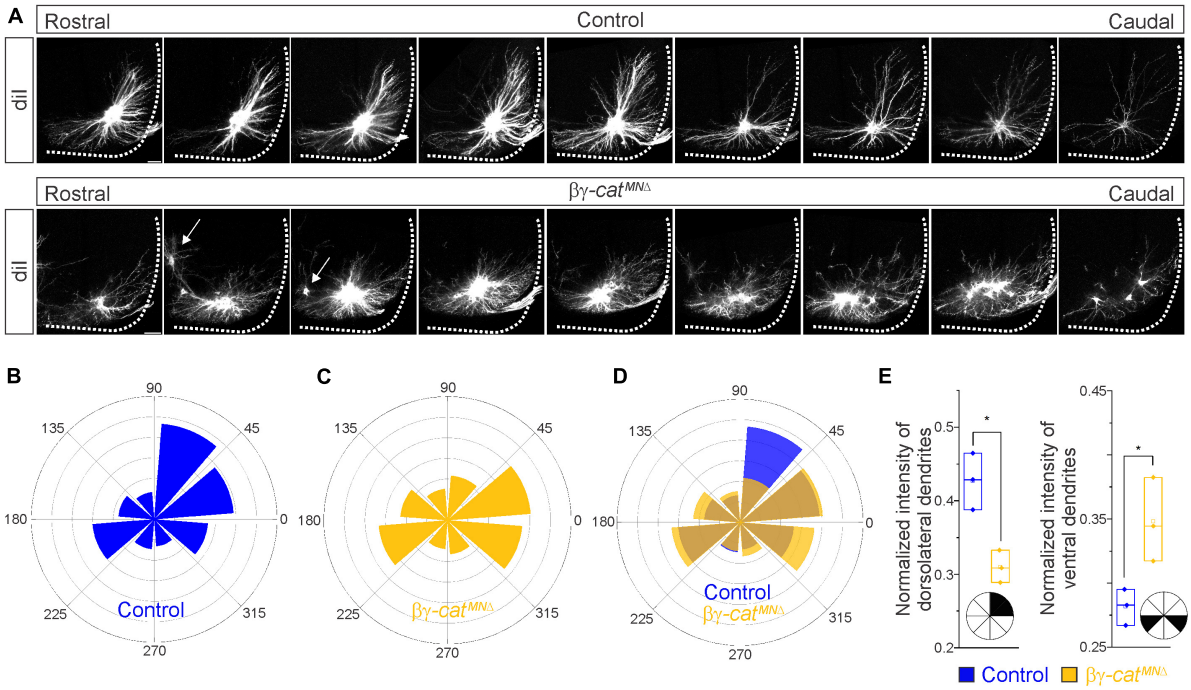

FIGURE 4
Catenins control phrenic MN dendritic growth and orientation. **(A)** Rostral to caudal extent of phrenic MN dendrites, as revealed by dil injections into the phrenic nerve in control and βγ-$cat^{MN\Delta}$ mice. Arrows indicate displaced phrenic MNs that remain close to the midline. Scale bar = 100 μm. **(B–D)** Radial plot of the normalized fluorescent intensity in each octant in control **(B,D)** and βγ-$cat^{MN\Delta}$ **(C,D)** mice. Zero degrees represents a line through the center of the phrenic MN cell bodies that is perpendicular to the midline. Dendrites in βγ-$cat^{MN\Delta}$ mice shift ventrally, with a loss of dorsolateral projections. **(E)** Quantification of the proportion of dendritic fluorescent intensity from 0 to 90° (left, dorsolateral) and from 180–225° and 315–360° (right, ventral) in control and βγ-$cat^{MN\Delta}$ mice. *$p < 0.05$.

respiratory populations in the brainstem, leading to the reduction in phrenic MN activation observed.

We then asked whether catenins might also play an analogous role in phrenic axon extension and arborization. We examined diaphragm innervation in control and βγ-$cat^{MN\Delta}$ mice at e18.5. We found that βγ-$cat^{MN\Delta}$ mice display a lack of innervation in the ventral diaphragm (Figure 5A, arrow), while the parts of the diaphragm that are innervated show a reduction in terminal arborization complexity (Figure 5A, star). Quantitation of total phrenic projections revealed a significant reduction in overall diaphragm innervation (Figures 5B, C). Collectively our data point to a catenin requirement for phrenic MN topography and axon and dendrite arborization, suggesting that these changes in early phrenic MN development lead to loss of phrenic MN activity and perinatal lethality due to respiratory insufficiency.

A narrow temporal requirement for catenin signaling in phrenic MN topography and function

Given the essential role for catenins in early phrenic MN development, we wanted to further understand the temporal dynamics of cadherin signaling, and asked whether sustained catenin expression is required for maintenance of the respiratory circuit. We used a *ChAT::Cre* promoter to specifically delete β- and γ-*catenin* in postmitotic MNs (β-*catenin flox/flox;* γ-*catenin flox/flox; ChAT::Cre*, referred to as βγ-$cat^{ChATMN\Delta}$ mice). βγ-$cat^{ChATMN\Delta}$ mice show MN-specific loss of catenin expression by e13.5 (Supplementary Figure 1D), survive to adulthood and do not display respiratory insufficiency or gasping at birth. We first assessed cell body position and found no changes between control and βγ-$cat^{ChATMN\Delta}$ mice (Figure 6A). Injecting dil into the phrenic nerve also revealed no differences in dendritic orientation between control and βγ-$cat^{ChATMN\Delta}$ mice (Figure 6B). To assess respiratory circuit function, we performed phrenic nerve recordings in isolated brainstem-spinal cord preparations in control and βγ-$cat^{ChATMN\Delta}$ mice at P4, and found that βγ-$cat^{ChATMN\Delta}$ mice exhibit similar phrenic MN bursting frequency, burst duration and overall activity as control mice (Figures 6C, D). Our data suggests that cadherins engage catenin signaling during a short temporal window early in development to shape respiratory motor output, but appear to be dispensable once early phrenic MN topography and morphology have been established.

Discussion

Phrenic MNs are a critical neuronal population that is essential for breathing, yet the molecular mechanisms that control their development and maintenance have remained elusive. Here, we show that β- and γ-catenin are required for phrenic MN organization, axonal and dendritic arborization, and respiratory output during a narrow developmental window. This requirement

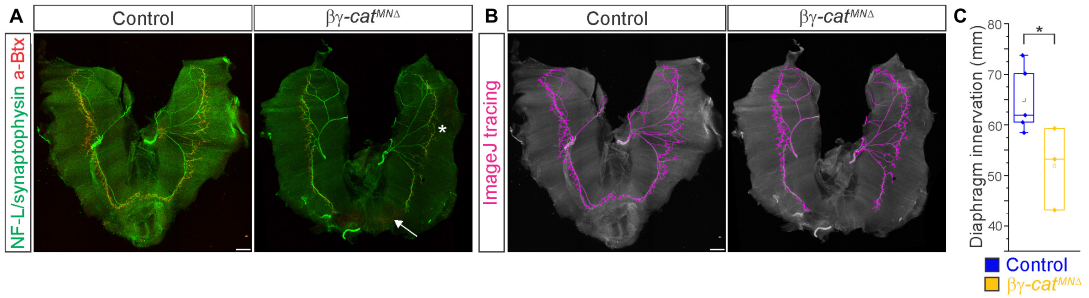

FIGURE 5
Catenins regulate phrenic MN axonal arborization. **(A)** Diaphragm innervation in control and βγ-$cat^{MN\Delta}$ mice. βγ-$cat^{MN\Delta}$ mice display a reduction in ventral diaphragm innervation (arrow) and arborization complexity (star) at e18.5. Motor axons are labeled in green (combination of neurofilament light chain/synaptophysin) and neuromuscular junctions in red (α-bungarotoxin, btx). Scale bar = 500 μm. **(B)** Phrenic projections were traced and quantified in ImageJ. **(C)** Quantification of diaphragm innervation in control and βγ-$cat^{MN\Delta}$ mice. *$p < 0.05$.

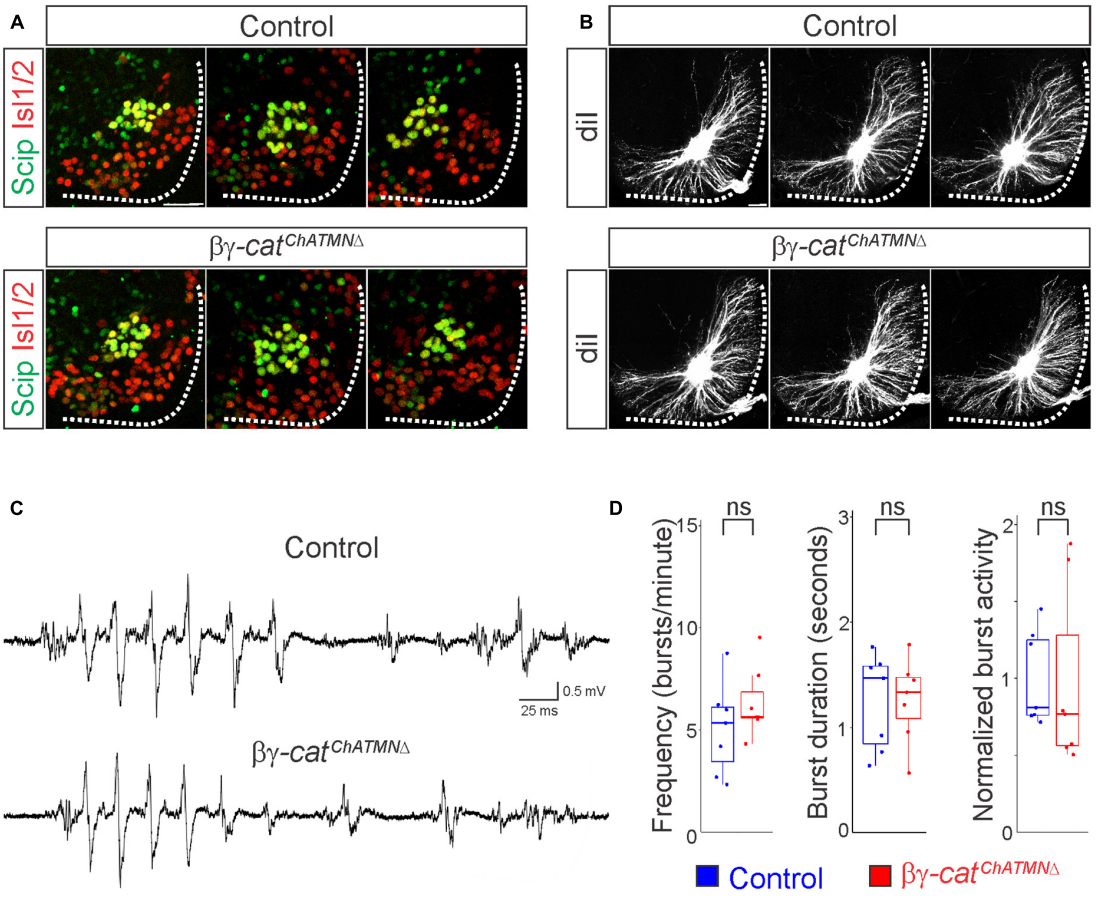

FIGURE 6
A narrow temporal requirement for catenin signaling in phrenic MN topography and function. **(A)** Examples of phrenic MN cell body distribution in control and βγ-$cat^{ChATMN\Delta}$ mice at e13.5. *ChAT::Cre*-mediated catenin deletion from postmitotic MNs does not affect their position or clustering. Scale bar = 25 μm. **(B)** DiI injections into the phrenic nerve reveal similar dendritic architecture in control and βγ-$cat^{ChATMN\Delta}$ mice at e18.5. Scale bar = 100 μm. **(C)** Representative suction electrode recordings from the phrenic nerve in P4 control and βγ-$cat^{ChATMN\Delta}$ mice show similar levels of phrenic MN activation. **(D)** Burst frequency, duration, and integrated activity are unchanged in βγ-$cat^{ChATMN\Delta}$ mice ($n = 7$ control, $n = 7$ βγ-$cat^{ChATMN\Delta}$ mice).

is likely due to their function in mediating cadherin adhesive interactions, as MN-specific cadherin inactivation results in similar defects (Vagnozzi et al., 2022). Although β-catenin also acts as a transcriptional activator in the Wnt signaling pathway, deletion of β-catenin alone does not impact phrenic MN development, suggesting that the role of catenins in respiratory function is independent of Wnt signaling (Vagnozzi et al., 2020). While catenins have a critical role in early phrenic MN development, they appear to be dispensable for maintaining the morphology and function of these MNs. Our findings indicate that distinct

molecular pathways are likely to mediate the establishment and maintenance of respiratory motor circuits at different timepoints throughout development and adulthood.

Catenins appear to be critical for phrenic MN organization. We find that catenin inactivation leads to both ventral shifts in PMC position and loss of clustering between cell bodies. While we observe similar shifts in cell body position when we inactivate 4 out of the 6 cadherins expressed in PMC neurons (cadherins N, 6, 9 and 10-$N^{MN\Delta}6910^{KO}$ mice), we do not see a loss of clustering in these mice (Vagnozzi et al., 2022). This could suggest that retaining expression of the remaining PMC-specific cadherins, 11 and 22, is sufficient to maintain the phrenic MN distinct tight clustering organization. Alternatively, our data could indicate that cell non-autonomous cadherin function plays a predominant role in MN clustering, and that eliminating cadherin signaling from all MNs leads to scattering and mixing of MN populations, causing disorganization not seen when solely eliminating PMC-specific cadherins. Despite differentially affecting PMC clustering, we observe similar changes in phrenic MN activity in $N^{MN\Delta}6910^{KO}$ and $\beta\gamma\text{-}cat^{MN\Delta}$ mice, suggesting that MN clustering may not significantly contribute to phrenic MN activity. Alternatively, since the loss of activity we observe in both mouse models is so severe, it may mask a subtler impact of clustering to PMC activity patterning and synchronization. Decoupling PMC clustering from changes in neuronal morphology and cell adhesion loss will help distinguish the contribution of each of these properties to respiratory motor output.

Our data show that cadherin signaling is required both for the elaboration of PMC axons and dendrites, however the impact of catenin inactivation on dendrites appears to be more severe. Phrenic MNs are able to elaborate axons in $\beta\gamma\text{-}cat^{MN\Delta}$ mice and axonal topography and orientation are mostly preserved, with some minor loss of terminal arborization. This loss of arborization might also lead to the observed reduction in phrenic MN numbers due to a lack of trophic support from the diaphragm. Dendrites however appear to be severely stunted, project haphazardly and their topography is lost. This indicates that cadherins have a much more predominant role in dendritic rather than axonal elaboration. While many signaling pathways contribute to phrenic axon growth and diaphragm innervation, including HGF/MET (Sefton et al., 2022), Slit/Robo (Charoy et al., 2017), and Col25a1 (Tanaka et al., 2014), to our knowledge, cadherins are the first cell adhesion molecules to be implicated in phrenic MN dendritic development.

Loss of catenin-mediated cadherin adhesive function results in a dramatic reduction of phrenic MN activity that leads to perinatal lethality. This could be due to the loss of descending inputs from brainstem respiratory centers that provide excitatory drive to initiate diaphragm contraction during inhalation. The dramatic change in PMC dendritic coordinates is likely to contribute significantly to the loss of presynaptic inputs and respiratory activity. Dendrites represent the largest surface area of neurons, and thus receive the majority of synaptic input. In sensory-motor circuits, proprioceptive inputs are primarily located on the dendrites of motor neurons, and different motor pools exhibit distinct, stereotyped patterns of dendritic arborization that contribute to sensory-motor specific connectivity (Vrieseling and Arber, 2006; Balaskas et al., 2019). This mode of cadherin action in respiratory circuits would be consistent with cadherin-dependent targeting mechanisms in the retina, where combinatorial codes of cadherin expression serve to direct axons and dendrites of synaptically connected neurons to their correct laminar targets (Osterhout et al., 2011; Duan et al., 2014, 2018).

In addition to establishing phrenic MN dendritic morphology, cadherins could directly contribute to phrenic connectivity through establishing a molecular recognition program between phrenic MN dendrites and pre-motor axons. Due to their restricted and selective expression in neural populations, cadherins are thought to function in circuit assembly by dictating synaptic specificity. Cadherin expression often reflects the functional connections formed in a circuit, suggesting they may represent a molecular code dictating the formation of selective synaptic connections (Suzuki et al., 1997). Cadherins are expressed on dendrites, axons, and growth cones of developing neurons (Basu et al., 2015) and have been visualized at synapses in both pre and postsynaptic compartments (Yamagata et al., 1995; Fannon and Colman, 1996; Uchida et al., 1996; Benson and Tanaka, 1998; Bozdagi et al., 2000; Manabe et al., 2000; Suzuki et al., 2007; Bartelt-Kirbach et al., 2010). Therefore, cadherins could function to establish respiratory neuron connectivity independently of their role in dictating axonal and dendritic targeting, at the level of the synapse, as it has been described in the hippocampus (Williams et al., 2011; Basu et al., 2017). Future experiments will determine the primary mode of cadherin action in respiratory circuit formation.

While early cadherin inactivation in MN progenitors results in dramatic changes in phrenic MN morphology and activity and leads to perinatal death, cadherin inactivation in postmitotic MNs does not impact respiratory output. This result provides initial evidence supporting a predominant role for cadherins in shaping dendritic orientation, as they appear to be dispensable once phrenic MN morphology has been established. Our findings indicate a model in which cadherins may function to direct the dendrites and axons of pre and postsynaptic neurons to the correct location, while additional cell adhesion molecules dictate synaptic connectivity. In support of this hypothesis, we have identified a number of cell adhesion molecules that are specifically expressed in phrenic MNs but are not required for their morphology. Our results also indicate that distinct mechanisms may function to maintain respiratory circuit integrity after initial formation. Understanding how these critical circuits are maintained in adulthood is essential, as loss of respiratory function underlies lethality in many neurodegenerative diseases such as Amyotrophic Lateral Sclerosis (ALS).

Data availability statement

The original contributions presented in this study are included in the article/**Supplementary material**, further inquiries can be directed to the corresponding author.

Ethics statement

This animal study was reviewed and approved by the Institutional Animal Care Use Committee of Case Western Reserve University (assurance number: A-3145-01, protocol number: 2015-0180).

Author contributions

AV and PP conceived the project and wrote the manuscript. AV, MM, RL, AA, LL, and PP performed the experiments and analyzed the data. NZ provided the reagents. All authors contributed to the article and approved the submitted version.

Funding

This work was funded by NIH R01NS114510 to PP, F30HD096788 to AV, T32GM007250 to AV/CWRU MSTP, and F31NS124240 to MM. PP is the Weidenthal Family Designated Professor in Career Development.

Acknowledgments

We thank Heather Broihier, Evan Deneris, Ashleigh Schaffer, Helen Miranda, and members of the Philippidou Lab for helpful discussions and Lin Mei for providing the β-catenin antibody.

Conflict of interest

The authors declare that the research was conducted in the absence of any commercial or financial relationships that could be construed as a potential conflict of interest.

Publisher's note

Supplementary material

The Supplementary Material for this article can be found online at: https://www.frontiersin.org/articles/10.3389/fncir.2023.1121049/full#supplementary-material

SUPPLEMENTARY FIGURE 1
Temporally controlled MN-specific catenin inactivation. **(a)** *Olig2::Cre*-mediated β- and γ-*catenin* inactivation results in downregulation of β- and γ-catenin in both MN progenitors (arrow) and MNs (arrowhead) at e11.5. β-catenin protein is visualized by antibody staining (green) while γ-*catenin* RNA by *in situ* hybridization (positive signal in black). MNs are labeled by Isl1/2 expression (red). **(b)** MN progenitor and phrenic MN distribution, but not numbers, are changed in βγ-$cat^{MN\Delta}$ mice at e11.5. MN progenitors are labeled by the expression of the TF Olig2, while phrenic MNs are labeled by the co-expression of Scip and Isl1/2. Levels of activated caspase 3 (green, right panels) do not significantly change in βγ-$cat^{MN\Delta}$ mice, although displaced cells close to the midline frequently appear to undergo apoptosis (arrow). **(c)** Quantitation of MN progenitors, phrenic MNs and apoptotic (caspase 3+) cells in βγ-$cat^{MN\Delta}$ mice at e11.5. Phrenic MNs were counted as the total number of Scip/Isl1/2+ cells at cervical levels of the spinal cord. MN progenitors and apoptotic cells were counted as the average number of Olig2+ and caspase 3+ cells, respectively, spanning 160 μm of the cervical spinal cord. **(d)** *ChAT::Cre*-mediated β- and γ-*catenin* inactivation results in downregulation of β- and γ-catenin in MNs (arrowhead) at e13.5. Scale bar = 50 μm.

References

Balaskas, N., Abbott, L. F., Jessell, T. M., and Ng, D. (2019). Positional strategies for connection specificity and synaptic organization in spinal sensory-motor circuits. *Neuron* 102, 1143.e4–1156.e4. doi: 10.1016/j.neuron.2019.04.008

Bartelt-Kirbach, B., Langer-Fischer, K., and Golenhofen, N. (2010). Different regulation of N-cadherin and cadherin-11 in rat hippocampus. *Cell Commun. Adhes.* 17, 75–82. doi: 10.3109/15419061.2010.549977

Basu, R., Duan, X., Taylor, M. R., Martin, E. A., Muralidhar, S., Wang, Y., et al. (2017). Heterophilic type II cadherins are required for high-magnitude synaptic potentiation in the hippocampus. *Neuron* 96, 160.e6–176.e8.

Basu, R., Taylor, M. R., and Williams, M. E. (2015). The classic cadherins in synaptic specificity. *Cell Adh. Migr.* 9, 193–201.

Bekirov, I. H., Nagy, V., Svoronos, A., Huntley, G. W., and Benson, D. L. (2008). Cadherin-8 and N-cadherin differentially regulate pre- and postsynaptic development of the hippocampal mossy fiber pathway. *Hippocampus* 18, 349–363. doi: 10.1002/hipo.20395

Benson, D. L., and Tanaka, H. (1998). N-cadherin redistribution during synaptogenesis in hippocampal neurons. *J. Neurosci.* 18, 6892–6904. doi: 10.1523/JNEUROSCI.18-17-06892.1998

Bozdagi, O., Shan, W., Tanaka, H., Benson, D. L., and Huntley, G. W. (2000). Increasing numbers of synaptic puncta during late-phase LTP: N-cadherin is synthesized, recruited to synaptic sites, and required for potentiation. *Neuron* 28, 245–259. doi: 10.1016/s0896-6273(00)00100-8

Brault, V., Moore, R., Kutsch, S., Ishibashi, M., Rowitch, D. H., McMahon, A. P., et al. (2001). Inactivation of the beta-catenin gene by Wnt1-Cre-mediated deletion results in dramatic brain malformation and failure of craniofacial development. *Development* 128, 1253–1264. doi: 10.1242/dev.128.8.1253

Chaimowicz, C., Ruffault, P. L., Cheret, C., Woehler, A., Zampieri, N., Fortin, G., et al. (2019). Teashirt1 (Tshz1) is essential for the development, survival and function of hypoglossal and phrenic motor neurons. *Development* 146:dev174045. doi: 10.1242/dev.174045

Charoy, C., Dinvaut, S., Chaix, Y., Morle, L., Sanyas, I., Bozon, M., et al. (2017). Genetic specification of left-right asymmetry in the diaphragm muscles and their motor innervation. *Elife* 6:e18481.

Demireva, E. Y., Shapiro, L. S., Jessell, T. M., and Zampieri, N. (2011). Motor neuron position and topographic order imposed by beta- and gamma-catenin activities. *Cell* 147, 641–652. doi: 10.1016/j.cell.2011.09.037

Dessaud, E., Yang, L. L., Hill, K., Cox, B., Ulloa, F., Ribeiro, A., et al. (2007). Interpretation of the sonic hedgehog morphogen gradient by a temporal adaptation mechanism. *Nature* 450, 717–720. doi: 10.1038/nature06347

Dewitz, C., Duan, X., and Zampieri, N. (2019). Organization of motor pools depends on the combined function of N-cadherin and type II cadherins. *Development* 146:dev180422. doi: 10.1242/dev.180422

Dewitz, C., Pimpinella, S., Hackel, P., Akalin, A., Jessell, T. M., and Zampieri, N. (2018). Nuclear Organization in the Spinal Cord Depends on Motor Neuron Lamination Orchestrated by Catenin and Afadin Function. *Cell Rep.* 22, 1681–1694. doi: 10.1016/j.celrep.2018.01.059

Duan, X., Krishnaswamy, A., De la Huerta, I., and Sanes, J. R. (2014). Type II cadherins guide assembly of a direction-selective retinal circuit. *Cell* 158, 793–807. doi: 10.1016/j.cell.2014.06.047

Duan, X., Krishnaswamy, A., Laboulaye, M. A., Liu, J., Peng, Y. R., Yamagata, M., et al. (2018). Cadherin combinations recruit dendrites of distinct retinal neurons to

a shared interneuronal scaffold. *Neuron* 99, 1145.e6–1154.e6. doi: 10.1016/j.neuron.2018.08.019

Esch, T., Lemmon, V., and Banker, G. (2000). Differential effects of NgCAM and N-cadherin on the development of axons and dendrites by cultured hippocampal neurons. *J. Neurocytol.* 29, 215–223. doi: 10.1023/a:1026515426303

Fannon, A. M., and Colman, D. R. (1996). A model for central synaptic junctional complex formation based on the differential adhesive specificities of the cadherins. *Neuron* 17, 423–434. doi: 10.1016/s0896-6273(00)80175-0

Greer, J. J. (2012). Control of breathing activity in the fetus and newborn. *Compr. Physiol.* 2, 1873–1888.

Greer, J. J., and Funk, G. D. (2005). Perinatal development of respiratory motoneurons. *Respir. Physiol. Neurobiol.* 149, 43–61. doi: 10.1016/j.resp.2005.03.017

Hirano, S., and Takeichi, M. (2012). Cadherins in brain morphogenesis and wiring. *Physiol. Rev.* 92, 597–634.

Li, X. M., Dong, X. P., Luo, S. W., Zhang, B., Lee, D. H., Ting, A. K., et al. (2008). Retrograde regulation of motoneuron differentiation by muscle beta-catenin. *Nat. Neurosci.* 11, 262–268.

Lowell, B., Olson, D., and Yu, J. (2006). Development and phenotype of ChAT-IRES-Cre mice. *MGI Direct Data Submission*

Machado, C. B., Kanning, K. C., Kreis, P., Stevenson, D., Crossley, M., Nowak, M., et al. (2014). Reconstruction of phrenic neuron identity in embryonic stem cell-derived motor neurons. *Development* 141, 784–794. doi: 10.1242/dev.097188

Manabe, T., Togashi, H., Uchida, N., Suzuki, S. C., Hayakawa, Y., Yamamoto, M., et al. (2000). Loss of cadherin-11 adhesion receptor enhances plastic changes in hippocampal synapses and modifies behavioral responses. *Mol. Cell Neurosci.* 15, 534–546. doi: 10.1006/mcne.2000.0849

Martinez-Garay, I. (2020). Molecular mechanisms of cadherin function during cortical migration. *Front. Cell Dev. Biol.* 8:588152. doi: 10.3389/fcell.2020.588152

Masai, I., Lele, Z., Yamaguchi, M., Komori, A., Nakata, A., Nishiwaki, Y., et al. (2003). N-cadherin mediates retinal lamination, maintenance of forebrain compartments and patterning of retinal neurites. *Development* 130, 2479–2494. doi: 10.1242/dev.00465

Osterhout, J. A., Josten, N., Yamada, J., Pan, F., Wu, S. W., Nguyen, P. L., et al. (2011). Cadherin-6 mediates axon-target matching in a non-image-forming visual circuit. *Neuron* 71, 632–639. doi: 10.1016/j.neuron.2011.07.006

Philippidou, P., Walsh, C. M., Aubin, J., Jeannotte, L., and Dasen, J. S. (2012). Sustained Hox5 gene activity is required for respiratory motor neuron development. *Nat. Neurosci.* 15, 1636–1644. doi: 10.1038/nn.3242

Price, S. R., De Marco Garcia, N. V., Ranscht, B., and Jessell, T. M. (2002). Regulation of motor neuron pool sorting by differential expression of type II cadherins. *Cell* 109, 205–216. doi: 10.1016/s0092-8674(02)00695-5

Riehl, R., Johnson, K., Bradley, R., Grunwald, G. B., Cornel, E., Lilienbaum, A., et al. (1996). Cadherin function is required for axon outgrowth in retinal ganglion cells in vivo. *Neuron* 17, 837–848.

Sefton, E. M., Gallardo, M., Tobin, C. E., Collins, B. C., Colasanto, M. P., Merrell, A. J., et al. (2022). Fibroblast-derived Hgf controls recruitment and expansion of muscle during morphogenesis of the mammalian diaphragm. *Elife* 11:e74592. doi: 10.7554/eLife.74592

Seong, E., Yuan, L., and Arikkath, J. (2015). Cadherins and catenins in dendrite and synapse morphogenesis. *Cell Adh. Migr.* 9, 202–213.

Suzuki, S. C., Furue, H., Koga, K., Jiang, N., Nohmi, M., Shimazaki, Y., et al. (2007). Cadherin-8 is required for the first relay synapses to receive functional inputs from primary sensory afferents for cold sensation. *J. Neurosci.* 27, 3466–3476. doi: 10.1523/JNEUROSCI.0243-07.2007

Suzuki, S. C., Inoue, T., Kimura, Y., Tanaka, T., and Takeichi, M. (1997). Neuronal circuits are subdivided by differential expression of type-II classic cadherins in postnatal mouse brains. *Mol. Cell Neurosci.* 9, 433–447. doi: 10.1006/mcne.1997.0626

Tanabe, K., Takahashi, Y., Sato, Y., Kawakami, K., Takeichi, M., and Nakagawa, S. (2006). Cadherin is required for dendritic morphogenesis and synaptic terminal organization of retinal horizontal cells. *Development* 133, 4085–4096. doi: 10.1242/dev.02566

Tanaka, T., Wakabayashi, T., Oizumi, H., Nishio, S., Sato, T., Harada, A., et al. (2014). CLAC-P/collagen type XXV is required for the intramuscular innervation of motoneurons during neuromuscular development. *J. Neurosci.* 34, 1370–1379. doi: 10.1523/JNEUROSCI.2440-13.2014

Tsuchida, T., Ensini, M., Morton, S. B., Baldassare, M., Edlund, T., Jessell, T. M., et al. (1994). Topographic organization of embryonic motor neurons defined by expression of LIM homeobox genes. *Cell* 79, 957–970.

Uchida, N., Honjo, Y., Johnson, K. R., Wheelock, M. J., and Takeichi, M. (1996). The catenin/cadherin adhesion system is localized in synaptic junctions bordering transmitter release zones. *J. Cell Biol.* 135, 767–779. doi: 10.1083/jcb.135.3.767

Vagnozzi, A. N., Garg, K., Dewitz, C., Moore, M. T., Cregg, J. M., Jeannotte, L., et al. (2020). Phrenic-specific transcriptional programs shape respiratory motor output. *Elife* 9;e52859. doi: 10.7554/eLife.52859

Vagnozzi, A. N., Moore, M. T., Lin, M., Brozost, E. M., Kc, R., Agarwal, A., et al. (2022). Coordinated cadherin functions sculpt respiratory motor circuit connectivity. *Elife* 11:e82116. doi: 10.7554/eLife.82116

Vrieseling, E., and Arber, S. (2006). Target-induced transcriptional control of dendritic patterning and connectivity in motor neurons by the ETS gene Pea3. *Cell* 127, 1439–1452. doi: 10.1016/j.cell.2006.10.042

Williams, M. E., Wilke, S. A., Daggett, A., Davis, E., Otto, S., Ravi, D., et al. (2011). Cadherin-9 regulates synapse-specific differentiation in the developing hippocampus. *Neuron* 71, 640–655. doi: 10.1016/j.neuron.2011.06.019

Yamagata, M., Herman, J. P., and Sanes, J. R. (1995). Lamina-specific expression of adhesion molecules in developing chick optic tectum. *J. Neurosci.* 15, 4556–4571. doi: 10.1523/JNEUROSCI.15-06-04556.1995

Yu, X., and Malenka, R. C. (2003). Beta-catenin is critical for dendritic morphogenesis. *Nat. Neurosci.* 6, 1169–1177.

Zhu, H., and Luo, L. (2004). Diverse functions of N-cadherin in dendritic and axonal terminal arborization of olfactory projection neurons. *Neuron* 42, 63–75. doi: 10.1016/s0896-6273(04)00142-4